ACS APPLIED MATERIALS & INTERFACES

Research Article

www.acsami.org

Carbon-Coated Magnetite Embedded on Carbon Nanotubes for Rechargeable Lithium and Sodium Batteries

Dae-Yeop Park and Seung-Taek Myung*

Department of Nano Science and Technology, Sejong University, 98 Gunja-dong, Gwangjin-gu, Seoul, 143-747, South Korea

ABSTRACT: Fe_3O_4, carbon-coated Fe_3O_4, and carbon-coated Fe_3O_4 embedded on carbon nanotubes are synthesized via hydrothermal reaction. Scanning electron microscopic analysis reveals that particle size of the as-synthesized Fe_3O_4 ranges 100−250 nm, whereas carbon-coated Fe_3O_4 ranges 10−15 nm in diameter and is surrounded by a thin carbon layer derived from sucrose. The surface modification by carbon is effective in prohibiting crystal growth during hydrothermal reaction. The carbon-coated Fe_3O_4 is loaded on conductive carbon nanotubes during a hydrothermal reaction where the carbon nanotubes are added prior to the reaction. Li and Na cell tests indicate that the carbon-coated Fe_3O_4 embedded on carbon nanotubes exhibits excellent capacity retention and a good rate capability compared to those of Fe_3O_4 and carbon-coated Fe_3O_4. For both cases, the presence of conductive carbon nanotubes provides a conduction path of electrons and is thereby responsible for good capacity retention. These results demonstrate the feasibility of dual alkali ions (Li^+ and Na^+) storage in inexpensive magnetite.

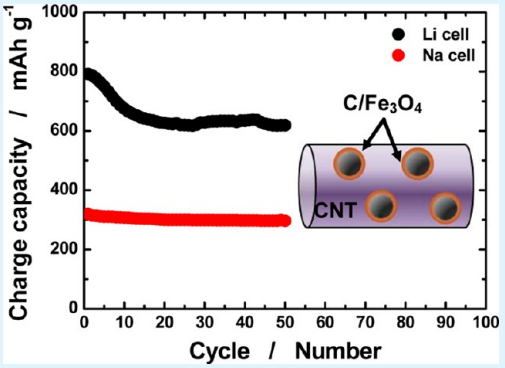

KEYWORDS: *magnetite, carbon nanotubes, conversion, negative electrode, batteries*

INTRODUCTION

Lithium-ion batteries used in portable devices provide us with an invaluable service in our day to day lives. Graphite is commonly used as a negative electrode material for lithium-ion batteries due to its stable cyclability and moderate capacity (theoretically 372 mAh g^{-1}). To meet the increasing demands of lithium-ion batteries, development of novel materials with better performance is of important concern. Of course, capacity and retention of active materials, such as metal, alloy, oxides, fluorides, and sulfides, should be considered. Among them, metal oxides are of interest because of their reactions related to the repetitive insertion−conversion process, enabling delivery of higher capacity greater than 600 mAh g^{-1}.[1−5] Among transition metal oxides,[6−15] iron oxide[16−20] is a promising negative electrode material in terms of material cost, non-toxicity, and abundance in nature. Moreover, Fe_3O_4 has a relatively high theoretical capacity of 928 mAh g^{-1},[16,20] which is greater than the theoretical capacity of conventional graphite, 372 mAh g^{-1}.[17] Although the high capacity driven by the conversion reaction is one of the main advantages of Fe_3O_4, there is a detrimental effect on capacity retention during the conversion reaction. Indeed, Li_2O formation causes poor cyclability because the produced Li_2O is intrinsically an electric insulator, so electron transfer is limited. For this reason, many investigations have focused on optimized synthetic routes, such as hydrothermal,[18−20] reflux methods,[21] coprecipitation,[22,23] and so on. Cheng et al.[21] synthesized Fe_3O_4/CNTs composites by using a reflux method, which can deliver a reversible capacity of 390 mAh g^{-1}. Behera et al.[22] also shows Fe_3O_4 to have an average size of under 20 nm through coprecipitation. The addition of sucrose seems to be effective in controlling the resulting particle size of Fe_3O_4.[19] Its application in practical lithium-ion batteries is hindered by poor cycling performance and large polarization. The electrochemical performances of Fe_3O_4 have been remarkably improved by carbon-coating or combining with other materials (such as carbon nanotube, graphene sheets), in particular Fe_3O_4-based nanocomposite.[24−36]

In this study, we attempt to synthesize Fe_3O_4 using a simple hydrothermal method. Since the reaction temperature is relatively low, the resulting product would have a small particle size. Carbon coating of the Fe_3O_4 particles can improve the resulting electric conductivity, which is expected to assist the conversion reaction easier to deliver high capacity. Hence, sucrose is added to yield carbon-coated Fe_3O_4. As mentioned-above, the appearance of Li_2O, byproduct formed during the conversion reaction, may exist among Fe_3O_4 or with converted Fe particles, and electron transfer can be limited by the presence of insulating Li_2O. To overcome the intrinsic problem of conversion reaction, carbon nanotubes (CNTs) are also added to further ensure electric conductivity assisted by the conductive CNTs. In addition, few reports have dealt with structural and electrochemical properties of Fe_3O_4 in Na cell.[37−39] We, here, present a facile synthesis of carbon-coated Fe_3O_4 embedded on CNTs. Also, we investigate the structure

Received: April 25, 2014
Accepted: July 7, 2014
Published: July 7, 2014

and electrochemical characteristics of the carbon-coated Fe_3O_4 embedded on CNTs in Li and Na cells as alkali ion storage.

EXPERIMENTAL SECTION

To synthesize Fe_3O_4, sodium acetate (3.6 g, Samchun) was first added in a solution mixture of ethylene glycol (35 mL, Junsei) and polyethylene glycol (PEG 400, 5 g, Samchun). Then, $FeCl_3{\cdot}6H_2O$ (1.35 g, Junsei) was added into the solution, and the resulting solution was continuously stirred for 30 min. The mixed solution was transferred into a Teflon-lined stainless autoclave (50 mL) and was hydrothermally reacted at 200 °C for 48 h to yield Fe_3O_4, followed by reactions:

$$FeCl_3{\cdot}6H_2O \rightarrow Fe^{3+} + 3HCl + 6OH^- + 6H^+ + 6e^- \quad (1)$$

$$Fe^{3+} + e^- \rightarrow Fe^{2+} + 2OH^- \rightarrow Fe(OH)_2 \quad (2)$$

$$Fe^{3+} + 3OH^- \rightarrow Fe(OH)_3 \rightarrow FeOOH + H_2O \quad (3)$$

$$2FeOOH + Fe(OH)_2 \rightarrow Fe_3O_4 + 2H_2O \quad (4)$$

For carbon-coating of Fe_3O_4, sucrose (0.005 mol, 0.1712 g, Samchun) was added together with $FeCl_3{\cdot}6H_2O$ into the solution mixture of ethylene glycol, polyethylene glycol, and sodium acetate. The solution was also transferred into a Teflon-lined stainless autoclave and hydrothermally treated at 200 °C for 48 h. Carbon nanotubes (1g, purchased from Hanwha nanotech) were dispersed in 200 mL of HNO_3 solution (60%, Junsei) with stirring for 12 h, and the black solution was diluted with distilled water for several times and filtered until pH reached neutral. The acid-treated powders were dried at 80 °C overnight. The treated CNTs (10 wt %) were dispersed in ethylene glycol followed by vigorous stirring for 2 h, and then, the $FeCl_3{\cdot}6H_2O$ with/without sucrose was added to black solution. The polyethylene glycol and sodium acetate (3.6 g, Samchun) were dissolved in the solution with continuously stirring for 30 min. The black solution was transferred into a Teflon-lined stainless autoclave (50 mL) and consequently hydrothermally treated at 200 °C for 48 h to produce carbon-coated Fe_3O_4 embedded on CNTs followed by the reaction mentioned above (reactions 1−4). After the reaction, the obtained precipitates were washed with ethanol and distilled water several times, and the resulting powders were dried at 80 °C for 24 h in air.

The synthesized products were characterized by X-ray diffraction (XRD, Rint-2000, Rigaku). The synthesized products were observed by scanning electron microscopy (SEM, S-4700, Hitachi) and transmission electron microscopy (TEM, JEM-3010, JEOL). An elemental analyzer (EA110, CE Instrument, Italy) was employed to determine the amount of carbon in the final products.

The synthesized powders were mixed with conductive carbon and polyacrylic acid[40] as binder, which shows good adhesion ability for conversion electrode, (8:1:1) in *N*-methyl-2-pyrrolidone (NMP). The slurry was applied onto a Cu foil and dried overnight at 80 °C in a vacuum oven. Electrochemical testing was performed in coin type R2032 cells. The counter electrode was lithium foil and the electrolyte solution was a 1 M $LiPF_6$ solution in ethylene carbonate (EC)/dimethyl carbonate (DMC) (3:7 ratio by volume). Working and counter electrodes were separated by a porous polypropylene film. For Na cell tests, sodium foil was used as a counter electrode. The electrolyte solution in sodium cell was a 1 M $NaClO_4$ solution in propylene carbonate (PC)/fluoroethylene carboncate, which fluorinates the surface of electrode, (FEC) (98:2 ratio by volume).[41] The glass microfiber filter was used as a separator. Cells were fabricated an Ar-filled glovebox. The prepared cells were tested with a galvanostatic mode in the operation range 0.5−2.5 V for Li cells and 0−2.5 V for Na cells at 25 °C.

The alternating current impedance measurements were performed with a Zahner Elektrik IM6 impedance analyzer over the frequency range from 1 MHz to 1 mHz with an amplitude of 10 mV at room temperature. To investigate the structural change during charge and discharge, cells were carefully disassembled in an Ar-filled glovebox, and the electrodes were washed with salt-free dimethyl carbonate overnight. Then, the electrodes were dried at 60 °C overnight in a vacuum oven. The recovered electrodes were wrapped with Mylar film in an Ar-filled glovebox to avoid contact with air during XRD measurement. In the same way, the recovered electrodes were ultrasonically dispersed in NMP for TEM measurements.

RESULTS AND DISCUSSION

Hydrothermal Synthesis of Fe_3O_4, Carbon-Coated Fe_3O_4, and Carbon-Coated Fe_3O_4 Embedded on CNTs.

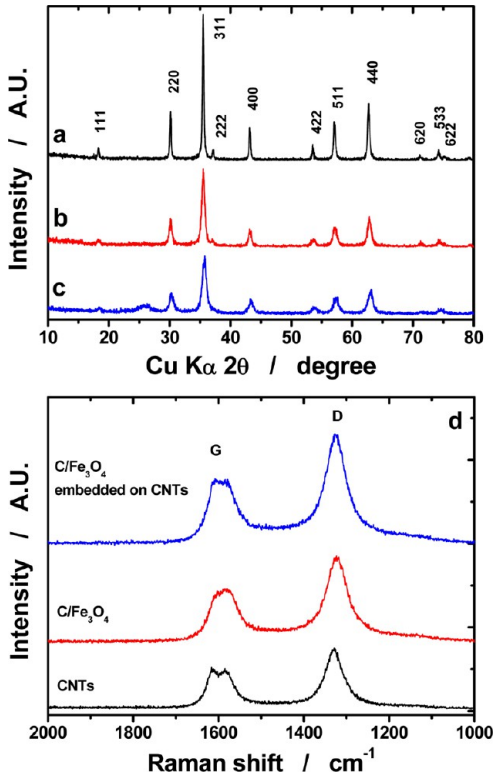

Figure 1. XRD patterns of hydrothermal products: (a) bare Fe_3O_4, (b) carbon-coated Fe_3O_4 (C/Fe_3O_4), (c) C/Fe_3O_4 embedded on CNTs (10 wt %). (d) Raman spectra of as-hydrothermally treated CNTs, C/Fe_3O_4 and C/Fe_3O_4 embedded on CNTs (10 wt %).

Figure 1 shows X-ray diffraction (XRD) patterns of as-synthesized Fe_3O_4, carbon-coated Fe_3O_4 (hereafter referred as to be C/Fe_3O_4), and C/Fe_3O_4 embedded on CNTs. The XRD pattern for the Fe_3O_4 (Figure 1a) indicates that the present hydrothermal treatment is simple and effective in obtaining highly crystalline Fe_3O_4 even though the reaction temperature was low, 200 °C. The crystal structure of the Fe_3O_4 belongs to cubic spinel with a $Fd\bar{3}m$ space group. For the C/Fe_3O_4 (Figure 1b), the relative intensity for the XRD pattern is slightly lower than that of the Fe_3O_4, and the widths of peaks are significantly broader than those of the Fe_3O_4. This implies that the carbon coating leads to a smaller particle size. Similarly, the hydrothermal treatment with CNTs retains detectable traces of CNTs at around 26° (2θ) (Figure 1c). There is no change for Fe_3O_4 phase in the XRD patterns before and after CNTs addition (10 wt %). Also, the crystal structure does not vary with the carbon coating and the addition of CNTs. Calculated lattice parameters for these products are approximately 8.388 Å, which is consistent with the value in literature.[24−36] Raman spectroscopic data are compared in Figure 1d. The hydro-

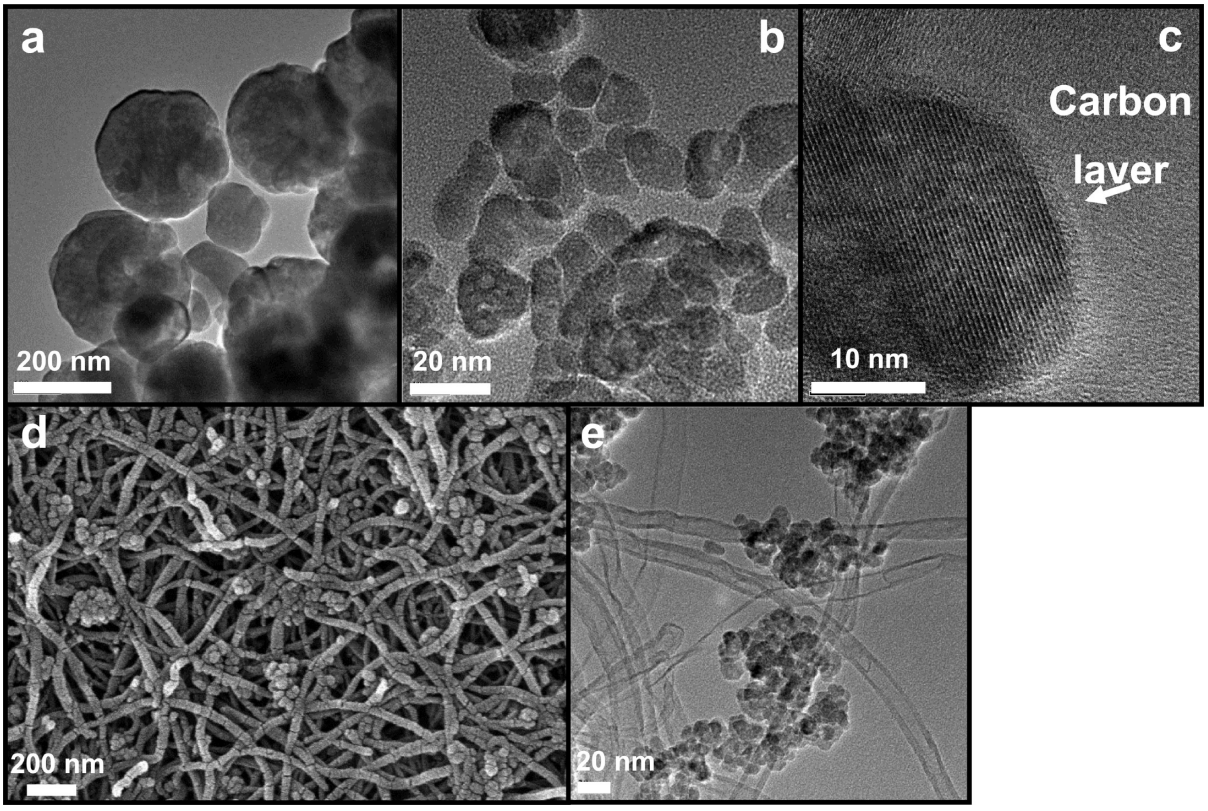

Figure 2. TEM images of (a) bare Fe_3O_4, (b) C/Fe_3O_4, (c) magnified image C/Fe_3O_4, (d) SEM image of C/Fe_3O_4 embedded on CNTs (10 wt %), and (e) the resulting TEM image of C/Fe_3O_4 embedded on CNTs (10 wt %).

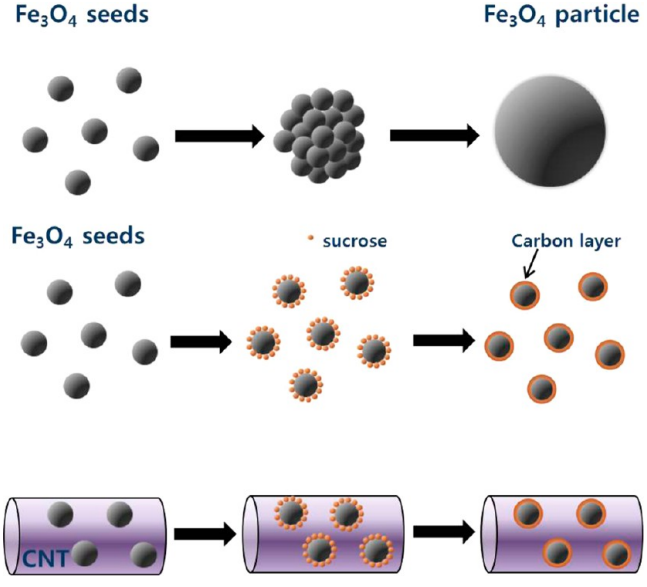

Figure 3. Schematic synthetic process of bare Fe_3O_4, C/Fe_3O_4, and C/Fe_3O_4 embedded on CNTs.

thermally treated CNTs show the typical reflection of carbon, except split of G-band around 1600 cm^{-1}. The produced C/Fe_3O_4 exhibits the presence of carbon, but the G-band spectrum does not split. The appearance of D- and G-bands indicates carbonization of sucrose during the given hydrothermal condition. Interestingly, the C/Fe_3O_4 embedded on CNTs features merged G-band of those of CNTs and C/Fe_3O_4. This information confirms the presence of carbon, which confirms the XRD data.

The presence of carbon is further evidenced by microscopy (Figure 2). The as-synthesized Fe_3O_4 shows spherical morphology, and the estimated particle size ranges from 100 to 250 nm in diameter (Figure 2a). For the C/Fe_3O_4, it is notable that the particle size of the Fe_3O_4 is significantly reduced, ranging 10−15 nm in diameter though agglomerated (Figure 2b). Magnified TEM image demonstrates that the Fe_3O_4 particle is surrounded by a thin carbon layer, of which the thickness approximates 2−3 nm (Figure 2c). The amount of carbon was determined to be about 0.2 wt %. Thus, advent of the broad XRD peaks in Figure 1b is ascribed to the presence of the nanosized Fe_3O_4 modified by a carbon layer. As CNTs were added, the C/Fe_3O_4 particles present only on the CNTs (Figures 2d and e). Elemental analysis result indicates that total amount of carbon including CNTs is approximately 10.1 wt % in the carbon-coated Fe_3O_4 embedded on CNTs. Crystal growth is natural even in a hydrothermal condition and the large Fe_3O_4 particles are perceived in Figure 2a. On the contrary, the carbon coating results in a dramatic decrease in the primary particle size. It is likely that, as soon as the crystal seeds of Fe_3O_4 are formed under the hydrothermal condition, the seeds are simultaneously encapsulated by sucrose in the solution and carbonization of the sucrose is consequently progressed (Figure 3). Since there is no possibility of contact among Fe_3O_4 seeds after the carbonization, particle growth such as carbon-free Fe_3O_4 would be inhibited. Also, the C/Fe_3O_4 particles have intimate contact with CNTs that have an intrinsically high electric conductivity. Nanosize particle formation process is schematically illustrated in Figure 3.

Electrochemical Properties of Fe_3O_4, Carbon-Coated Fe_3O_4, and Carbon-Coated Fe_3O_4 Embedded on CNTs in Li Cells. Produced powders, Fe_3O_4, C/Fe_3O_4, and C/Fe_3O_4

dx.doi.org/10.1021/am502424j | ACS Appl. Mater. Interfaces 2014, 6, 11749−11757

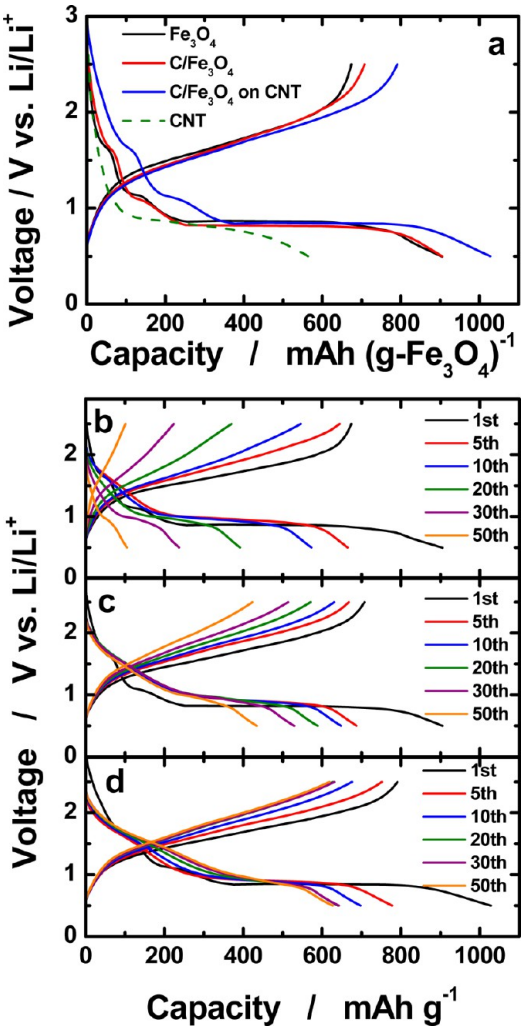

Figure 4. (a) First discharge (reduction) and charge (oxidation) curves of bare Fe_3O_4, C/Fe_3O_4, C/Fe_3O_4 embedded on CNTs (10 wt %), and CNTs in Li cells; continuous discharge and charge curves of (b) bare Fe_3O_4, (c) C/Fe_3O_4, and (d) C/Fe_3O_4 embedded on CNTs (10 wt %). Tests were performed in galvanostatic mode by applying a constant current of 50 mA g^{-1} in the voltage range 2.5−0.5 V at 25 °C.

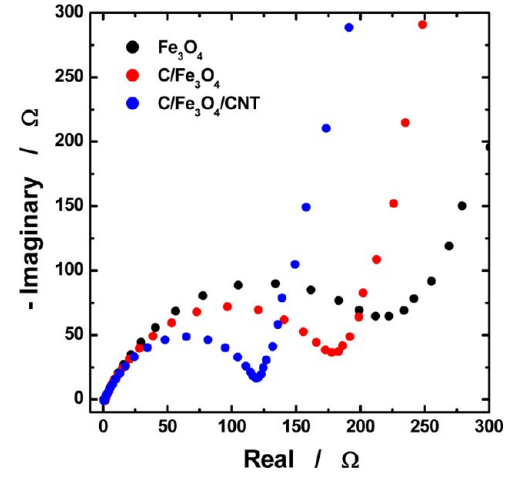

Figure 5. Ac-impedance plots for the fresh cells composed of bare Fe_3O_4, C/Fe_3O_4, and C/Fe_3O_4 embedded on CNTs (10 wt %) electrodes in Li cells.

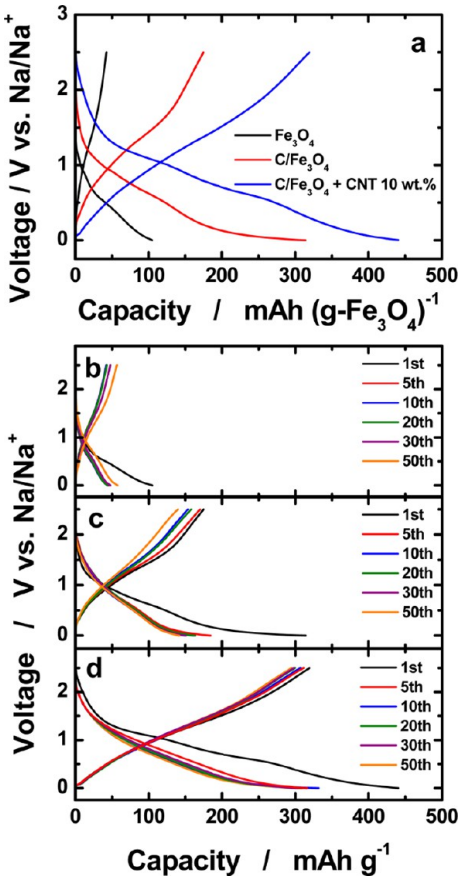

Figure 6. (a) First discharge (reduction) and charge (oxidation) curves of bare Fe_3O_4, C/Fe_3O_4, and C/Fe_3O_4 embedded on CNTs (10 wt %) in Na cells; continuous discharge and charge curves of (b) bare Fe_3O_4, (c) C/Fe_3O_4, and (d) C/Fe_3O_4 embedded on CNTs (10 wt %). Tests were performed in galvanostatic mode by applying a constant current of 50 mA g^{-1} in the voltage range 2.5−0.01 V at 25 °C.

embedded on CNTs, were electrochemically tested in galvanostatic mode by applying a constant current of 50 mA g^{-1} in the voltage range 2.5−0.5 V at 25 °C. Both Fe_3O_4 and C/Fe_3O_4 electrodes exhibit a large discharge (reduction) capacity of about 900 mAh g^{-1} (Figure 4a), accompanied by three distinct voltage plateaus, 1.63, 1.12, and 0.88 V for lithiation. The reaction dominant above 0.88 V would be ascribed to Li^+ intercalation into the Fe_3O_4 framework: $Fe_3O_4 + 2Li^+ + 2e^- \rightarrow Li_2Fe_3O_4$.[30] Then, a long voltage plateau, presumably associated with a conversion reaction appears: $Li_2Fe_3O_4 + 6Li^+ + 6e^- \rightarrow 3Fe + 4Li_2O$. Upon charging (oxidation), those distinct plateaus are not obvious, but the resulting curve is sloppy. The C/Fe_3O_4 delivers slightly higher capacity (700 mAh g^{-1} compared with the Fe_3O_4 (670 mAh g^{-1}), presumably due to the presence of carbon on the surface of Fe_3O_4, which is expected to assist electron transfer, or due to the conversion reaction occurring in nanoparticles.

The addition of CNTs is indeed effective in increasing capacity. The discharge capacity reaches 1030 mAh g^{-1} for the C/Fe_3O_4 embedded on CNTs (10 wt %) in Figure 4a. The additional capacity to 0.9 V would be related to decomposition of electrolyte and formation of solid electrolytic interfaces on the surface of CNTs, and the added CNTs somehow allow Li^+ insertion below 0.8 V, which may be overlapped with the main conversion reaction of Fe_3O_4. The overcapacity in the region

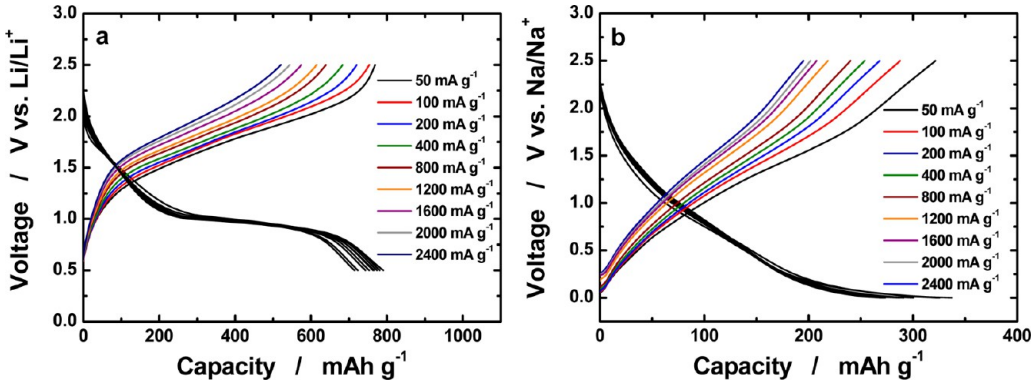

Figure 7. Rate capability of C/Fe_3O_4 embedded on CNTs (10 wt %) electrodes tested in (a) Li and (b) Na cells.

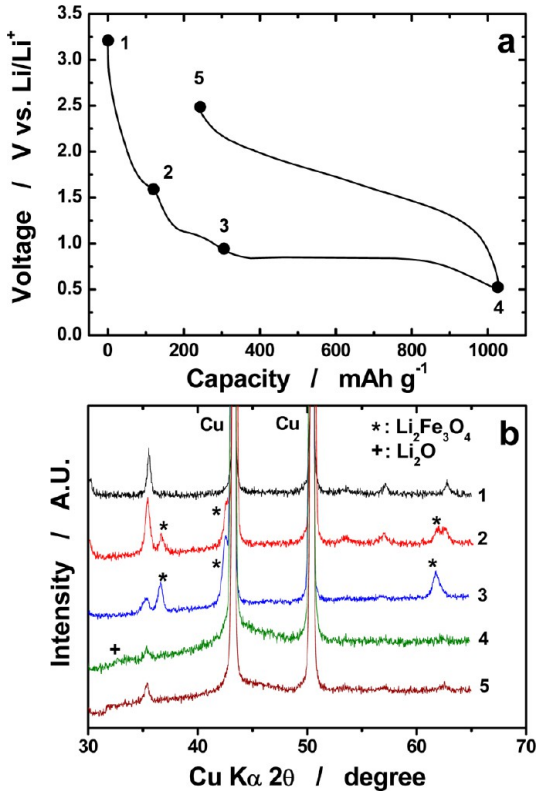

Figure 8. (a) First discharge−charge curve of C/Fe_3O_4 embedded on CNTs (10 wt %) electrodes tested in Li cell. The closed circles indicate the points that XRD measurements were conducted; (b) ex-situ XRD patterns of C/Fe_3O_4 embedded on CNTs (10 wt %) electrode.

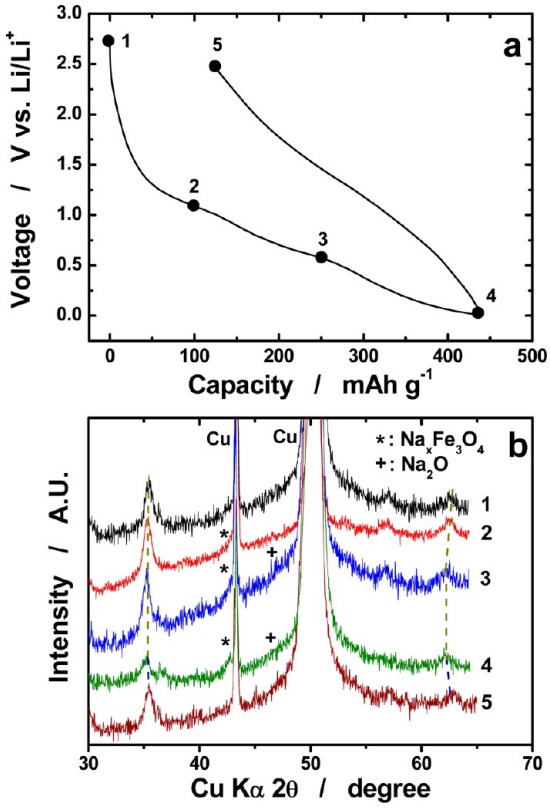

Figure 9. (a) First discharge−charge curve of C/Fe_3O_4 embedded on CNTs (10 wt %) electrodes tested in Na cell. The closed circles indicate the points that XRD measurements were conducted; (b) ex situ XRD patterns of C/Fe_3O_4 embedded on CNTs (10 wt %) electrode.

would be ascribed to Li^+ insertion into the CNTs. Therefore, the discharge capacity exceeding the theoretical capacity of Fe_3O_4 (928 mAh g^{-1}) is understood. The resulting efficiency of the electrode is approximately 78% for the C/Fe_3O_4 embedded on the CNTs, whereas those of the Fe_3O_4 and C/Fe_3O_4 are calculated to be 74% and 78%, respectively. These facts indicate that the formation of C/Fe_3O_4 embedded on CNTs is effective in improvement of capacity.

Continuous discharge−charge curves reveal the C/Fe_3O_4 electrode's obviously better capacity retention than Fe_3O_4, showing about 59% retention of the first charge capacity for the C/Fe_3O_4 and 15% retention for the Fe_3O_4 (Figures 4b and c). This capacity fade indicates difficulty of the conversion reaction. Namely, the repeated structural change from the spinel structure to metal may cause tremendous stress in the host structure on every cycle. Meanwhile, the addition of CNTs results in a notable improvement in the capacity associated with the conversion upon cycling, retaining 78% of the first charge capacity (Figure 4d). Since cyclability of the employed CNTs is very poor, a capacity loss up to an initial 10 cycles would reflect the capacity fade of the CNTs.

Figure 5 shows ac-impedance plots for the fresh electrodes of Fe_3O_4, C/Fe_3O_4, C/Fe_3O_4 embedded on CNTs in Li cells. The data clarify that the presence of carbon coating and CNTs is effective in reducing resistance. Note that the C/Fe_3O_4 particles are attached on the conducting CNTs (Figures 2d and e). It is most likely that, although the electric insulating Li_2O is formed via the conversion reaction, the formed Fe particles, as a result

dx.doi.org/10.1021/am502424j | ACS Appl. Mater. Interfaces 2014, 6, 11749−11757

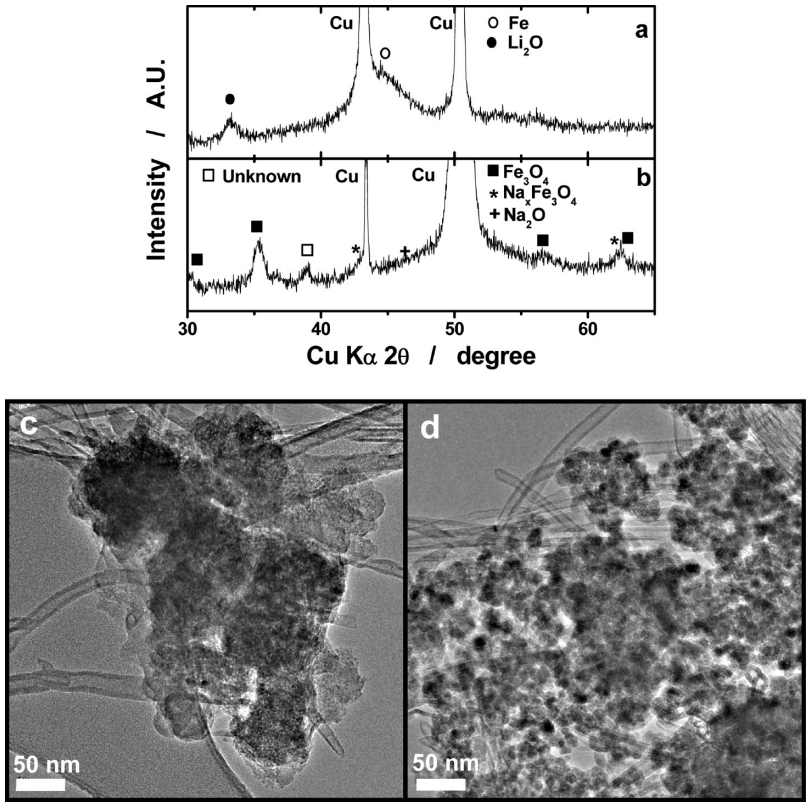

Figure 10. XRD patterns of C/Fe_3O_4 embedded on CNTs (10 wt %) electrodes tested in (a) Li and (b) Na cells; TEM images of the cycled C/Fe_3O_4 embedded on CNTs (10 wt %) electrodes tested in (c) Li and (d) Na cells.

of the conversion reaction, would reside on the conducting CNTs, which are likely to act as paths for electron transfer. Thus, the embedment of Fe_3O_4 on CNTs results in better cyclability compared to the Fe_3O_4 and C/Fe_3O_4. This visible variation in impedance clearly explains the importance of electrically conducting CNTs to maintain high capacity during the repetitive conversion reaction.

Electrochemical Properties of Fe_3O_4, Carbon-Coated Fe_3O_4 and Carbon-Coated Fe_3O_4 Embedded on CNTs in Na Cells. Applicability of Fe_3O_4 toward anodes for Na batteries are recently introduced by Komaba et al.[37] and more recently by Balaya et al.[38] Because of the good electrode performances modified by the conducting carbons shown in (Figures 3−5), the produced composites electrode would show similar performances via conversion reaction in Na cells. Sodium cells were fabricated using the prepared powders (Fe_3O_4, C/Fe_3O_4, and C/Fe_3O_4 embedded on CNTs). They were electrochemically tested in galvanostatic mode by applying a constant current of 50 mA g^{-1} at 25 °C in the voltage range 0−2.5 V vs Na/Na^+, because standard electrode potential of sodium is about 0.3 V lower than lithium. In case of the bare Fe_3O_4, it is disappointing that the first discharge capacity is approximately 104 mAh g^{-1} (Figure 6a). Compared to the results in Li cell, the resulting capacity decreases dramatically in the Na cell. Also, discharge capacity is only 40 mAh g^{-1}. It is attributed to the fact that Na ions does not completely react with Fe_3O_4 upon cycling (Figure 6b), probably due to large particle size (Figure 2a). Meanwhile, the C/Fe_3O_4 exhibits better activity in Na electrolyte. The differences are that the resulting particle size is small (Figure 2b) and the surface is modified by sucrose-derived carbons (Figure 2c). The first discharge capacity is 310 mAh g^{-1}, and the charge capacity delivered is about 175 mAh g^{-1}, retaining 85% of the first charge capacity upon cycling (Figure 6c).

The results demonstrate the importance of particle size and the presence of carbon for de/sodiation. Surprisingly, the reversible capacity increases further for the C/Fe_3O_4 embedded on CNTs. As a result, the delivered capacities are approximately 440 mAh g^{-1} for the first discharge and 321 mAh g^{-1} for the first charge (Figure 6a), showing 73% Coulombic efficiency, which is close to the results obtained in the Li cell (Figure 4a). It is also interesting to mention that the capacity retention is approximately 93% upon cycling (Figure 6d), in which the retention was 78% for the same electrode in the Li cell (Figure 4d). As reported earlier by Komaba et al.,[37] Fe_3O_4 is active in the voltage range 1.5−4 V vs Na/Na^+. In the present study, we investigated the C/Fe_3O_4 embedded on CNTs in the range 0−2.5 V vs Na/Na^+. Balaya et al.[38] also tested Fe_3O_4 supported by carbon marix, and they suggested a high charge capacity of about 350 mAh g^{-1}, but it showed drastic capacity fade within 10 cycles. In this case, Na^+ insertion into the amorphous carbon spontaneously causes gradual disintegration of the carbon structure because of repetitive insertion of the larger Na^+ ions into the less established diffusion channel of the amorphous carbon the capacity fade. In the present experiment, the Na^+ insertion reaction into the CNTs seems to be difficult because of the larger ionic size of Na^+ (1.02 Å), so that there is no gradual capacity fading during earlier 10 cycles (Figure 6d) unlike the results of Balaya et al.,[38] implying that the reaction is solely related to de/sodiation of Fe_3O_4 supported by conducting CNTs.

Rate Performances of C/Fe_3O_4 Embedded on CNTs in Li and Na Cells. Rate capability was measured for the C/Fe_3O_4 embedded on CNTs varying current from 50 mA g^{-1} to

2400 mA g^{-1} on charge in Li and Na electrolyte (Figure 7). Prior to charge, all cells were subjected to discharge at a constant current of 50 mA g^{-1}. For the Li cell, the cell delivers a charge capacity of about 785 mAh g^{-1} at 50 mA g^{-1}, and the cell is still markedly active even at a high current (2400 mA g^{-1}) showing 520 mAh g^{-1} (Figure 7a). Similar to the Li cell, the Na cell also displays a good rate performance at a high current: 196 mAh g^{-1} at 2400 mA g^{-1} (Figure 7b), which is superior to that of a hard carbon in Na cell.[42] This performance is notable because metal oxides based on conversion reactions show poor electrochemical properties due to insulating Li_2O or Na_2O caused by conversion reactions and structure destruction from repetitive structure change. These impede movement of Na or Li ions and electrons. Here, the nanosized primary particle C/Fe_3O_4 would be an important factor in improving the rate capability because the shortened diffusion path makes Li^+ diffusion easier. In addition, despite the presence of insulating Li_2O and Na_2O, these products reside on the electro-conducting CNTs. Therefore, the Fe_3O_4 could exhibit reasonable rate capability. These results demonstrate that the electro-conducting CNTs and the nanosized C/Fe_3O_4 play an important role in transferring electrons so as to achieve high rate capability in both Li and Na cells.

Structural Analyses of Extensively Cycled Electrodes of Carbon-Coated Fe_3O_4 Embedded on CNTs in Li and Na Cells. The Fe_3O_4 electrode was examined by XRD so as to follow structural evolution during electrochemical reaction in Li and Na cells. *Ex-situ* XRD measurements were made at a specific position marked by the closed circles (Figure 8a). The as-fabricated electrode exhibits the original Fe_3O_4 spinel structure (Figure 8b-1). At 1.6 V, a new phase, $Li_2Fe_3O_4$, is perceived, which is evidence of Li^+ insertion into the Fe_3O_4 spinel framework (Figure 8b-2), preferentially entering 16*d* sites in the initial stage ($x < 1$ in $Li_xFe_3O_4$).[30] The $Li_2Fe_3O_4$ phase further evolves as Li^+ insertion progresses (Figure 8b-3), in which the empty 8*a* and 48*f* sites are filled before initiation of conversion reaction, transforming to $Li_2Fe_3O_4$ hierarchically. At the end of discharge ($Li_8Fe_3O_4$), the strong reflections of Fe_3O_4 and $Li_2Fe_3O_4$ are greatly diminished and a broad hill appears in the range 40−48° (2θ) (Figure 8b-4). In addition, a broad peak is also perceived at around 33° (2θ). This abrupt reduction in the diffraction intensity is usually observed in conversion reaction.[43] Structure is rearranged because of the formation of metal from metal oxide, and the resulting converted product shows low crystallinity ascribed to an irregular ordering of metal atoms. Here, the broad hill in the XRD pattern coincides with the converted Fe metal. The broad peak around 33° (2θ) is the trace of Li_2O, which elucidates the occurrence of the conversion reaction. On charge, the broad hill appeared at the end of discharge turns out to be quite flattened in the range 40−48° (2θ) (Figure 8b-5). This is because Fe metal is also oxidized to Fe_3O_4, probably an amorphous phase. Also, the original spinel phase is recovered, confirming the reversibility of conversion reaction. This is another indication of the reversibility of the conversion reaction in which the formed Li_2O on discharge is dissolved and is not observed in the XRD pattern (Figure 8b-5).

For Na cell, ex situ XRD measurements were also made to follow the structural change during sodiation and desodiation of Fe_3O_4 (Figures 9a and b). As sodiation is progressed (point 2 in Figure 9a), a shoulder peak, $Na_xFe_3O_4$ phase suggested by Komaba et al.,[37] appears at around 43° (2θ) where it overlapped with the Cu current collector peak (Figure 9b-2). The formation of $Na_xFe_3O_4$ indicates occurrence of Na^+ insertion into empty 8*a*, 16*d*, and 48*f* sites of Fe_3O_4. It is further supported from the pattern that the peaks shift toward lower angle compared to those as-synthesized (Figure 9b-1). The phase is further developed at point 3, and the diffraction peaks shift further toward low angle, accompanied by lattice expansion as a consequence of Na^+ insertion. Inversion of peak intensity between Fe_3O_4 and $Na_xFe_3O_4$, which was dominant for Li^+ insertion process (Figure 8b-3), is not observed for the reaction in Na cell, presumably owing to difficulty of the larger Na^+ insertion into the oxide framework though being progressed. By contrast, the Na_2O phase although weak is perceived at 46° (2 θ) as a result of progress of conversion reaction in the XRD pattern, at which Li_2O was not found at the same capacity (250 mAh g^{-1}) in Li cell (Figure 8b-3). This indicates that the large Na^+ insertion into the spinel structure is not possible anymore. Instead, conversion reaction becomes dominant below the point (Figure 9b-4). No change in the peak positions but reduction in the peak intensity suggests the conversion the reaction undergoes in the region. Similar to the Li system, the phase is recovered to the original Fe_3O_4 structure (Figure 9b-5), indicating a reversible insertion−conversion process.

Extensively cycled electrodes were examined by XRD and TEM to understand the structural integrity of C/Fe_3O_4 embedded on CNTs in Li and Na cells (Figure 10). Since the electrochemical reaction occurs based on the conversion reaction, all electrodes are subject to experience structural rearrangement from Fe_3O_4 to Fe metal. The phase transformation to Fe metal causes significant stress to the oxide lattice during electrochemical reduction. In this process, oxygen is released from the Fe_3O_4 oxide lattice, and the oxygen bonds with Li^+ or Na^+ to form Li_2O or Na_2O. As demonstrated in Figure 8b, the newly formed Fe metal has a low crystallinity or amorphous character. Hence, although the Fe metal is charged (oxidized), the resulting oxide also has low crystallinity (Figure 8b-5). These reactions are repeated upon cycling. As a result, the electrode cycled in Li cell displays Fe (44° (2θ) and Li_2O (33° (2θ)) reflections (Figure 10a). Indeed, carbon-coated Fe_3O_4 nanoparticles are loaded on the highly conductive CNTs. Insulating Li_2O is detrimental for capacity retention, whereas the presence of CNTs is likely to compensate for electron transfer which was perturbed by the Li_2O. For this reason, the C/Fe_3O_4 embedded on CNTs is able to retain its high capacity upon cycling, though the crystalline structure was transformed to an amorphous one (Figure 10a). Compared to the fresh Fe_3O_4 (Figures 2b and c), which exhibited a smooth surface and edge (Figure 2), morphology of the cycled Fe_3O_4 is severely damaged and the smooth surface is not observed anymore (Figure 10c).

As is clear from the XRD pattern (Figure 10b), the original Fe_3O_4 phase is still maintained after the extensive cycling test in Na cell. Compared to the result shown in Figure 10a, it is surprising that the structure could be retained even after the repetitive conversion reaction. As discussed in Figure 9b, Na^+ insertion does not readily occur because of the larger ionic radius of Na^+. To complete the conversion reaction, the empty Fe_3O_4 sites should be filled to form $Na_2Fe_3O_4$ eventually, and then, the conversion reaction would occur via the reaction: $Na_2Fe_3O_4 + 6Na^+ + 6e^- \rightarrow 3Fe + 4Na_2O$, similar to the reaction in the Li cell. In consideration of the first discharge capacity 440 mAh g^{-1}, only 47.44% of Fe_3O_4 was utilized via the above reaction to participate in the electrochemical

reaction: insertion−conversion process. Namely, 52.6% of Fe_3O_4 remains as intact because of the diffuculty of large Na^+ insertion into the Fe_3O_4 framwork as is confirmed in the TEM image of extensively cycled powders (Figure 10d), compared to Figure 2d.

Although the original particles are disintegrated via the rearrangement of crystal structure during conversion reaction, those nanoparticles are still attached on the CNTs. This, in turn, facilitates electron movements so that the high capacity could be retained during cycling in Li and Na cells (Figures 4 and 6). Recent reports by Yoon et al.[30] and Oh et al.[39] also emphasize that their C/Fe_3O_4 using pitch as the carbon source could have good cyclability with high capacity in Li and Na cells, respectively. Since the carbon coating was made at a high temperature, the crystalline carbon would aim to transfer electrons readily, which correlates with our results. Therefore, introduction of conducting materials on active materials is a necessary condition to facilitate electron transfer and, thereby, the accomplishment of high capacity retention and better rate capability substantially in both Li and Na cells.

CONCLUSIONS

In summary, the CNTs addition to the nanosized C/Fe_3O_4 produce a composite of C/Fe_3O_4 embedded on CNTs. Improvement of electrode performance mainly stems from the presence of the electrically conductive CNTs that allow ready transfer of electrons during the conversion reaction in both Li and Na cells, though overcapacity was seen due to Li^+ insertion into the CNTs. The C/Fe_3O_4 embedded on CNTs could retain the high capacity upon cycling in both Li cell (620 mAh g^{-1} at 50th cycle with 78% capacity retention) and Na cell (298 mAh g^{-1} at 50th cycle with 93% capacity retention). In particular, the delivered charge capacities are sufficiently high at various rates: 516 mAh g^{-1} at 2400 mA g^{-1} for the Li cell and 196 mAh g^{-1} at 2400 mA g^{-1} for the Na cell. The present modification would be applicable for various kinds of metal oxides, negative electrode materials that are encountered with conversion reaction, and may improve electrode performances such as capacity retention and rate capability, in particular, for rechargeable Na batteries.

AUTHOR INFORMATION

Corresponding Author

*Tel: 82 2 3408 3454. Fax: 82 2 3408 4342. Email: smyung@sejong.ac.kr.

Notes

The authors declare no competing financial interest.

ACKNOWLEDGMENTS

This study was partly supported by grants from the National Research Foundation of Korea funded by the Korean government (MEST) (NRF-2009-C1AAA001-0093467) and Basic Science Research Program through the National Research Foundation of Korea (NRF) funded by the Ministry of Education, Science and Technology (NRF-2011-0024683).

REFERENCES

(1) Peled, E.; Menachem, C.; Bar-Tow, D.; Melman, A. Improved Graphite Anode for Lithium-Ion Batteries: Chemically Bonded Solid Electrolyte Interface and Nanochannel Formation. *J. Electromhem. Soc.* **1996**, *143*, L4−L7.

(2) Yoshio, M.; Wang, H.; Fukada, K.; Hara, Y.; Adachi, Y. Effect of Carbon Coating on Electrochemical Performance of Treated Natural Graphite as Lithium-Ion Battery Anode Material. *J. Elctrochem. Soc.* **2000**, *147*, 1245−1250.

(3) Wang, H.; Yoshio, M.; Abe, T.; Ogumi, Z. Characterization of Carbon-Coated Natural Graphite as a Lithium-Ion Battery Anode Material. *J. Elctrochem. Soc.* **2002**, *149*, A499−A503.

(4) Buiel, E.; Dahn, J. R. Li-Insertion in Hard Carbon Anode Materials for Li-Ion Batteries. *Electrochim. Acta* **1999**, *45*, 121−130.

(5) Hu, J.; Li, H.; Huang, X. Electrochemical Behavior and Microstructure Variation of Hard Carbon Nano-Spherules As Anode Material for Li-Ion Batteries. *Solid State Ionics* **2007**, *178*, 265−271.

(6) Laruelle, S.; Grugeon, S.; Poizot, P.; Dolle, M.; Dupont, L.; Tarascon, J.-M. On the Origin of the Extra Electrochemical Capacity Displayed by MO/Li Cells at Low Potential. *J. Electrochem. Soc.* **2002**, *149*, A627−A634.

(7) Poizot, P.; Laruelle, S.; Grugeon, S.; Dupont, L.; Tarascon, J.-M. Nano-Sized Transition-Metal Oxides as Negative-Electrode Materials for Lithium-Ion Batteries. *Nature* **2000**, *407*, 496−499.

(8) Xia, Q.; Zhao, H.; Du, Z.; Wang, J.; Zhang, T.; Wang, J.; Lv, P. Synthesis and Electrochemical Properties of MoO_3/C Composite as Anode Material for Lithium-Ion Batteries. *J. Power Sources* **2013**, *226*, 107−111.

(9) Tao, T.; Glushenkov, A. M.; Zhang, C.; Zhang, H.; Zhou, D.; Guo, Z.; Liu, H. K.; Chen, Q.; Hu, H.; Chen, Y. MoO_3 Nanoparticles Dispersed Uniformly in Carbon Matrix: A High Capacity Composite Anode for Li-Ion Batteries. *J. Mater. Chem.* **2011**, *21*, 9350−9355.

(10) Bhaskar, A.; Deepa, M.; Rao, T. N.; Varadaraju, U. V. Enhanced Nanoscale Conduction Capability of a MoO_2/Graphene Composite for High Performance Anodes in Lithium Ion Batteries. *J. Power Sources* **2012**, *216*, 169−178.

(11) Nakazawa, H.; Sano, K.; Abe, T.; Baba, M.; Kumagai, N. Charge−Discharge Characteristics of All-Solid-State Thin-Filmed Lithium-Ion Batteries Using Amorphous Nb_2O_5 Negative Electrodes. *J. Power Sources* **2007**, *174*, 838−842.

(12) Myung, S.-T.; Takahashi, N.; Komaba, S.; Yoon, C. S.; Sun, Y.-K.; Amine, K.; Yashiro, H. Nanostructured TiO_2 and its Application in Lithium-Ion Storage. *Adv. Funct. Mater.* **2011**, *21*, 3231−3241.

(13) Tepavcevic, S.; Xiong, H.; Stamenkovic, V. R.; Zuo, X.; Balasubramanian, M.; Prakapenka, V. B.; Johnson, C. S.; Rajh, T. Nanostructured Bilayered Vanadium Oxide Electrodes for Rechargeable Sodium-ion Batteries. *ACS Nano* **2012**, *6*, 530−538.

(14) Armstrong, A. R.; Armstrong, G.; Canales, J.; Bruce, P. G. TiO_2-B Nanowires. *Angew. Chem., Int. Ed.* **2004**, *43*, 2286−2288.

(15) Kim, J.; Chung, M. K.; Ka, B. H.; Ku, J. H.; Park, S.; Ryu, J.; Oh, S. M. The Role of Metallic Fe and Carbon Matrix in Fe_2O_3/Fe/Carbon Nanocomposite for Lithium-Ion Batteries. *J. Elctrochem. Soc.* **2010**, *157*, A412−A417.

(16) Kang, E.; Jung, Y. S.; Cavanagh, A. S.; Kim, G. H.; George, S. M.; Dillon, A. C.; Kim, J. K.; Lee, J. Fe_3O_4 Nanoparticles Confined in Mesocellular Carbon Foam for High Performance Anode Materials for Lithium-Ion Batteries. *Adv. Funct. Mater.* **2011**, *21*, 2430−2438.

(17) Duan, H.; Gnanaraj, J.; Liang, J. Synthesis and Rate Performance of Fe_3O_4-Based Cu Nanostructured Electrodes for Li Ion Batteries. *J. Power Sources* **2011**, *196*, 4779−4784.

(18) Deng, H.; Li, X.; Peng, Q.; Wang, X.; Chen, J.; Li, Y. Monodisperse Magnetic Single-Crystal Ferrite Microspheres. *Angew. Chem., Int. Ed.* **2005**, *44*, 2782−2785.

(19) Sun, X.; Zheng, C.; Zhang, F.; Yang, Y.; Wu, G.; Yu, A.; Guan, N. Size-Controlled Synthesis of Magnetite (Fe_3O_4) Nanoparticles Coated with Glucose and Gluconic Acid from a Single Fe(III) Precursor by a Sucrose Bifunctional Hydrothermal Method. *J. Phys. Chem. C* **2009**, *113*, 16002−16008.

(20) Ni, S.; He, D.; Yang, X.; Li, T. Low Temperature Synthesis of Fe_3O_4 Nanoparticles and its Application in Lithium ion Batteries. *Mater. Chem. Phys.* **2011**, *130*, 1260−1264.

(21) Cheng, J. P.; Yu, J.; Shi, D.; Wang, D. S.; Liu, Y. F.; Liu, F.; Zhang, X. B.; Li, J. G. Controllable One-Step Synthesis of Magnetite/Carbon Nanotubes Composite and its Electrochemical Properties. *Appl. Phys. A: Mater. Sci. Process.* **2012**, *106*, 837−842.

(22) Behera, S. K. Facile Synthesis and Electrochemical Properties of Fe_3O_4 Nanoparticles for Li Ion Battery Anode. *J. Power Sources* **2011**, *196*, 8669−8674.
(23) He, Y.; Huang, L.; Cai, J.-S.; Zheng, X.-M.; Sun, S.-G. Structure and Electrochemical Performance of Nanostructured Fe_3O_4/Carbon Nanotube Composites as Anodes for Lithium Ion Batteries. *Electrochim. Acta* **2010**, *55*, 1140−1144.
(24) Jin, S.; Deng, H.; Long, D.; Liu, X.; Zhan, L.; Liang, X.; Qiao, W.; Ling, L. Facile Synthesis of Hierarchically Structured Fe_3O_4/Carbon Micro-Flowers and Their Application to Lithium-Ion Battery Anodes. *J. Power Sources* **2011**, *196*, 3887−3893.
(25) Wang, L.; Yu, Y.; Chen, P. C.; Zhang, D. W.; Chen, C. H. Electrospinning Synthesis of C/Fe_3O_4 Composite Nanofibers and Their Application for High Performance Lithium-Ion Batteries. *J. Power Sources* **2008**, *183*, 717−723.
(26) Muraliganth, T.; Murugan, A. V.; Manthiram, A. Facile Synthesis of Carbon-Decorated Single-crystalline Fe_3O_4 Nanowires andTheir Application as High Performance Anode in Lithium Ion Batteries. *Chem. Commun.* **2009**, *47*, 7360−7362.
(27) Cui, Z. M.; Jiang, L. Y.; Song, W. G.; Guo, Y. G. High-Yield Gas−Liquid Interfacial Synthesis of Highly Dispersed Fe_3O_4 Nanocrystals and Their Application in Lithium-Ion Batteries. *Chem. Mater.* **2009**, *21*, 1162−1166.
(28) Zhou, G.; Wang, D. W.; Li, F.; Zhang, L.; Li, N.; Wu, Z. S.; Wen, L.; Lu, G. Q.; Cheng, H. M. Graphene-Wrapped Fe_3O_4 Anode Material with Improved Reversible Capacity and Cyclic Stability for Lithium Ion Batteries. *Chem. Mater.* **2010**, *22*, 5306−5313.
(29) Joint Committee on Powder Diffraction Standards; File No. JCPDS Card, 88-0315.
(30) Kim, H. S.; Baek, S. H.; Jang, M. W.; Sun, Y. K.; Yoon, C. S. Fe-Fe_3O_4 Composite Electrode for Lithium Secondary Batteries. *J. Electromhem. Soc.* **2012**, *159*, A325−A329.
(31) Wang, B. B.; Wang, G.; Zheng, Z. Z.; Bai, J. T.; Bai, J. B. Carbon Coated Fe_3O_4 Hybrid Material Prepared by Chemical Vapor Deposition for High Performance Lithium-Ion Batteries. *Electrochim. Acta* **2013**, *106*, 235−243.
(32) Jin, B.; Liu, A.-H.; Liu, G.-Y.; Yang, Z.-Z.; Zhong, X.-B.; Ma, X.-Z.; Wang, H.-Y. Fe_3O_4-Pyrolytic Graphite Oxide Composite as an Anode Material for Lithium Secondary Batteries. *Electrochim. Acta* **2013**, *90*, 426−432.
(33) Zhang, J. J.; Yao, Y.; Huang, T.; Yu, A. S. Uniform Hollow Fe_3O_4 Spheres Prepared by Template-Free Solvothermal Method as Anode Material for Lithium-Ion Batteries. *Electrochim. Acta* **2012**, *78*, 502−507.
(34) Li, M.-Y.; Wang, Y.; Liu, C.-L.; Gao, H.; Dong, W.-S. Iron Oxide/Carbon Microsphere Lithium-Ion Battery Electrode with High Capacity and Good Cycling Stability. *Electrochim. Acta* **2012**, *67*, 187−193.
(35) Xiong, Q. Q.; Tu, J. P.; Lu, Y.; Chen, J.; Yu, Y. X.; Qiao, Y. Q.; Wang, X. L.; Gu, C. D. Synthesis of Hierarchical Hollow-Structured Single-Crystalline Magnetite (Fe_3O_4) Microspheres: The Highly Powerful Storage Versus Lithium as an Anode for Lithium Ion Batteries. *J. Phys. Chem. C* **2012**, *116*, 6495−6502.
(36) Huang, Y. D.; Dong, Z. F.; Jia, D. Z.; Guo, Z. P.; Cho, W. I. Preparation and Characterization of Core−Shell Structure Fe_3O_4/C Nanoparticles with Unique Stability and High Electrochemical Performance for Lithium-Ion Battery Anode Material. *Electrochim. Acta* **2011**, *56*, 9233−9239.
(37) Komaba, S.; Mikumo, T.; Yabuuchi, N.; Ogata, A.; Yoshida, H.; Yamada, Y. Electrochemical Insertion of Li and Na Ions into Nanocrystalline Fe_3O_4 and α-Fe_2O_3 for Rechargeable Batteries. *J. Electrochem. Soc.* **2010**, *157*, A60−A65.
(38) Hariharan, S.; Saravanan, K.; Ramar, V.; Balaya, P. A. Rationally Designed Dual Role Anode Material for Lithium-Ion and Sodium-Ion Batteries: Case Study of Eco-friendly Fe_3O_4. *Phys. Chem. Chem. Phys.* **2013**, *15*, 2945−2953.
(39) Oh, S.-M.; Myung, S.-T.; Yoon, C. S.; Lu, J.; Hassoun, J.; Scrosati, B.; Amine, K.; Sun, Y.-K. Advanced $Na[Ni_{0.25}Fe_{0.5}Mn_{0.25}]O_2$/C-$Fe_3O_4$ Sodium-Ion Batteries Using EMS Electrolyte for Energy Storage. *Nano Lett.* **2014**, *14*, 1620−1626.
(40) Komaba, S.; Shmonura, K.; Yabuuchi, N.; Ozeki, T.; Yui, H.; Konno, K. Study on Polymer Binders for High-Capacity SiO Negative Electrode of Li-Ion Batteries. *J. Phys. Chem. C* **2011**, *115*, 11487−13495.
(41) Komaba, S.; Murata, W.; Ishikawa, T.; Yabuuchi, N.; Ozeki, T.; Nakayama, T.; Ogata, A.; Gotoh, K.; Fujiwara, K. Electrochemical Na Insertion and Solid Electrolyte Interphase for Hard-Carbon Electrodes and Application to Na-Ion Batteries. *Adv. Funct. Mater.* **2011**, *21*, 3859−3867.
(42) Ponrouch, A.; Goni, A. R.; Palacin, M. R. High Capacity Hard Carbon Anodes for Sodium Ion Batteries in Additive Free Electrolyte. *Electrochem. Commun.* **2013**, *27*, 85−88.
(43) Myung, S.-T.; Sakurada, S.; Yashiro, H.; Sun, Y.-K. Iron Trifluoride Synthesized via Evaporation Method and Its Application to Rechargeable Lithium Batteries. *J. Power Sources* **2013**, *223*, 1−8.